Mathematical-morphology-based edge detectors for detection of thin edges in low-contrast regions

J.-A. Jiang, C.-L. Chuang, Y.-L. Lu and C.-S. Fahn

Abstract: A new edge detector based on mathematical morphology to preserve thin edge features in low-contrast regions as well as other apparent edges is proposed. A quad-decomposition edge enhancement process, a thresholding process, and a mask-based noise filtering process were developed and used to enhance thin edge features, extract edge points and filter out some meaningless noise points, respectively. Moreover, five bipolar oriented edge masks were also designed to remove most of the incorrectly detected edge features. Many experiments were conducted to evaluate and compare the performance of the proposed algorithm and several conventional ones. Pratt's figure of merit achieved by the proposed algorithm was as high as 92.5. The comprehensive experimental results show that the proposed algorithm is capable of preserving thin edge details successfully in low-contrast regions and is robust against noise.

1 Introduction

Edge detection is a fundamental and essential pre-processing step in applications such as image segmentation and computer vision, because edges represent important contour features in the corresponding image. Over the years, many approaches have been proposed to extract the contour features in an image. For example, the Sobel detector [1] used local gradient operators, which were capable of detecting edges having high spatial frequencies and certain orientations only. The Sobel detector produced poor results when the edges in an image were burred and noisy. The Prewitt operator [2] was proposed to extract contour features by fitting a least-squares-error (LSE) quadratic surface over a 3×3 image window and differentiate the fitted surface. The Canny edge detector [3] was a multiple-stage algorithm, which used Gaussian convolution technique first to smooth the image, and then measured the gradient properties in the image by a set of Robert's cross convolution masks. The Laplacian operator [3] used a second-order differential operator to find edge points based on the zero-crossing properties of the processed edge points.

Most of the previously proposed edge detectors were based on utilising a set of convolution masks to treat the image, and then applying a global threshold to transform the image into a binary edge image for further processing. When a global threshold was applied to extract the edge points in an image, a common disadvantage found in the above-mentioned approaches was that some thin edge details in the image were eliminated, for example, fine intensity differences in low-contrast regions (where the brightness was too dark or too bright). However, fine intensity differences in the image might represent important contour features. The further processing algorithms might perform poorly or misconduct the results improperly if these thin edge details were pruned.

Mathematical morphology theory [4] has been utilised as the basic theory of many newly proposed edge detectors for distinguishing contour features in an image. Trujillo [5] used a 3×3 mask to produce a gradient image to extract the contour features of an image, which is somewhat similar to the morphological residue edge detector. However, Trujillo's edge detector may misclassify some undesired edge features. Chen *et al.* [6] proposed a pseudo top-hat mathematical morphological operator to extract thin edge features of an image with reasonable performance. Chanda *et al.* [7] proposed a modified morphology-based edge detector, but it can capture only contour features with some specific orientation, and the extracted edge features might be fractal or discontinuous. Many other researches also found that the mathematical morphology theory was very useful in many image and video processing applications, such as image matching [8, 9] and video de-interlacing [10]. Hence, the morphological dilation residue edge detector was utilised to extract the contour features in this work.

In this work, a novel mathematical-morphology-based edge detector is proposed to extract thin edge features in the low contrast regions of an image. This paper is organised as follows: Section 2 describes the proposed edge detection algorithm based on mathematical morphology. Section 3 proposes four edge enhancement cases for sharpening thin edge details in low contrast regions. The bipolar oriented edge masks applied to erase noisy pixels are described in Section 4. Comprehensive comparisons between the proposed algorithm and other existing edge

doi:10.1049/iet-ipr:20060273

Paper first received 5th September 2006 and in final revised form 5th April 2007

J.-A. Jiang and C.-L. Chuang are with the Department of Bio-Industrial Mechatronics Engineering, National Taiwan University, Taipei 106, Taiwan, Republic of China

Y.-L. Lu and C.-S. Fahn are with the Department of Computer Science and Information Engineering, National Taiwan University of Science and Technology, Taipei 106, Taiwan, Republic of China

C.-L. Chuang is also with the Institute of Biomedical Engineering, National Taiwan University, Taipei 106, Taiwan, Republic of China

E-mail: jajiang@ntu.edu.tw

detection approaches are presented in Section 5. Conclusions are given in Section 6.

2 Proposed morphological edge detector

2.1 General descriptions

The main goal of this work is to develop an algorithm which can detect and preserve thin edge features in the low-contrast regions of an image. In this work, we utilise a morphological top-hat contrast enhancement operator to increase the pixel intensity differences in the image. Therefore, we can obtain an edge image with better quality using a morphological dilation residue edge detector. However, when the thin edge features are present in low-contrast regions, the strengths of pixel intensity differences are very weak and are probably undetectable by a global threshold. Therefore, the edge image is divided into several sub-images using the quad-decomposition technique proposed by Samet *et al.* [11, 12]. Next, the pixel intensity differences in each sub-image are enhanced by means of referring to the mean and standard deviation of the edge strength in the corresponding sub-image. Since the entire fine contour features are enhanced, a global threshold is then applied to transform the edge image into a binary image. Moreover, five bipolar oriented edge masks are applied to remove incorrectly detected edge pixels and reduce noisy pixels in the final resulting image. The overall procedure for the proposed algorithm is illustrated in Fig. 1.

2.2 Morphological contrast enhancement

As shown in Fig.1, the proposed algorithm consists of five steps. The first and second steps are based on the mathematical morphological operations. Let F and B denote the original image set and the structuring element set, respectively.

To increase the contrast level of the original image F, the morphological contrast enhancement process is applied to F to increase the pixel intensity differences cooperating with a star structuring element B as shown in Fig. 2. The contrast enhancement is

$$F_c = F + \mathrm{WTH}(F) - \mathrm{BTH}(F) \tag{1}$$

where F_c is the contrast-enhanced image derived from the original image F, and $\mathrm{WTH}(F)$ and $\mathrm{BTH}(F)$ are the white and the black top-hat transformations of original image F,

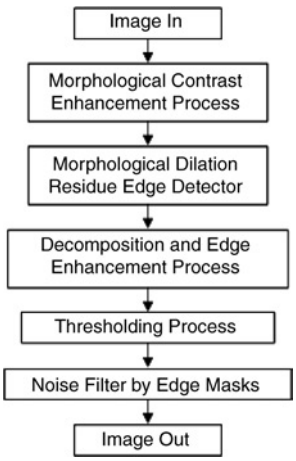

Fig. 1 *Conceptual block diagram of the proposed morphological edge detection algorithm*

Fig. 2 *Structuring element for contrast enhancement and dilation residue edge detection*

respectively. The definitions of operations $\mathrm{WTH}(F)$ and $\mathrm{BTH}(F)$ are given as

$$\mathrm{WTH}(F) = F - (F \circ B) \tag{2}$$

$$\mathrm{BTH}(F) = (F \bullet B) - F \tag{3}$$

where the operators $\circ$ and $\bullet$ are the mathematical morphological opening and closing operators defined in [13, 14], respectively. The primary goal of the contrast enhancement process is to accentuate and sharpen the features in the image. This process makes the original image more useful for visualisation, and also makes it easier to perform post-processing of the image.

2.3 Morphological dilation residue edge detector

The morphological dilation residue edge detector is applied to the contrast-enhanced image F_c to extract the contour feature details of the original image F. The detector is

$$F_e = (F_c \oplus B) - F_c \tag{4}$$

where F_e represents the extracted contour features that contain edges with various strengths. The symbol $\oplus$ represents the mathematical morphological dilation operator, which is defined in [13–14].

Although the contrast level of the original image F has been enhanced before detecting the edge features in the image, some smooth edges in the low-contrast regions are still too weak to be detected if a global threshold value is applied to F_e for extracting edge points. To prevent thin contour details from being removed by thresholding F_e, it is necessary to develop a technique to enhance them. In the following two sections, a recursive quad-decomposition process and a set of edge enhancements are applied to F_e to strengthen the smooth edges in low-contrast regions. Moreover, another set of bipolar oriented edge masks are also used to remove noise after the thresholding process.

3 Quad-decomposition edge enhancement

As mentioned in the Section 2.3, if the level of brightness in the entire original image F is not well distributed, the extracted contour features F_e might contain edges with various strengths. When we apply a global threshold value to F_e, many contour features in the regions that are too bright or too dark might be undetectable and be eliminated from the final result of edge extraction. Therefore, enhancing some meaningful smooth edges is needed before thresholding F_e. In this section, a new contour feature enhancement strategy based on a quad-decomposition technique is proposed and discussed.

The quad-decomposition, proposed by Samet *et al.* [11, 12], is a process that recursively decomposes an image into four sub-images with equal size, as shown in Fig. 3. This process stops when side lengths of the sub-images (width or height) reach the user-defined shortest side lengths. In this process, four edge point enhancement cases are defined to distinguish sub-images that contain meaningful smooth edge features. Before performing enhancement in each sub-image, the mean value and

Fig. 3 *Illustration of quad-decomposition of an image*

standard deviation of each sub-image are calculated from

$$\mu_\alpha = \frac{\sum_{i=1}^{M_\alpha} \sum_{j=1}^{N_\alpha} F_\alpha(i,j)}{M_\alpha \times N_\alpha} \tag{5}$$

$$\delta_\alpha = \sqrt{\frac{\sum_{i=1}^{M_\alpha} \sum_{j=1}^{N_\alpha} [F_\alpha(i,j) - \mu_\alpha]^2}{M_\alpha \times N_\alpha}} \tag{6}$$

where F_α is the αth sub-image obtained from dividing the extracted contour features F_e. M_α and N_α are the width and height of the sub-image F_α, and μ_α and δ_α are the mean value and standard deviation of the sub-image F_α, respectively.

On the basis of μ_α and δ_α of each sub-image F_α, one of four pixel enhancement methods, described later, is selected and applied to F_α to enhance the thin contour features in the corresponding region in F_e. Every pixel $P_\alpha(i,j)$ in position (i,j) in sub-image F_α should be processed by the proposed edge pixel enhancement operators. The criteria for these processes are summarised in Table 1 and defined in detail in the following subsections.

3.1 Redundant background

For a pixel for which the grey level value $P_\alpha(i,j)$ is less than the mean value μ_α of its related sub-image F_α and the sub-image F_α has $\mu_\alpha < 2$ and $\delta_\alpha < 2$, then the pixel is considered to be a background pixel and is pruned to grey level 0 (i.e. black).

3.2 Thin edges enhancement

For a pixel for which the grey level value $P_\alpha(i,j)$ is greater than the mean value μ_α of its related sub-image F_α and less than $\mu_\alpha + 1.5 \times \delta_\alpha$ and the sub-image F_α has $\mu_\alpha < 2$ and $\delta_\alpha < 2$, then the pixel is considered to be a thin edge pixel and is set to the square of $P_\alpha(i,j)$ [i.e. $P_\alpha(i,j)^2$].

3.3 Intensive thin edges enhancement

For a pixel for which the grey level value $P_\alpha(i,j)$ is greater than $\mu_\alpha + 1.5 \times \delta_\alpha$ and less than $\mu_\alpha + 3 \times \delta_\alpha$ and its associated sub-image F_α has $\mu_\alpha < 2$ and $\delta_\alpha < 2$, then the pixel is considered to be an intensive thin edge pixel and is set to the cube of $P_\alpha(i,j)$ [i.e. $P_\alpha(i,j)^3$].

3.4 Thin edges in complex background enhancement

For a pixel for which the grey level value $P_\alpha(i,j)$ is greater than $\mu_\alpha + 1.5 \times \delta_\alpha$ and its related sub-image F_α has $\mu_\alpha > 5$ and $\delta_\alpha > 6$, then the pixel is considered to be a thin edge pixel in a complex background and is set to the square of $P_\alpha(i,j)$ [as $P_\alpha(i,j)^2$].

The values of the mean and the deviation specified in Table 1 are determined experimentally, and are specially for treating gradient images, such as the contour feature image F_e. We have utilised many sample pictures to achieve the best estimation on the values of these condition parameters. The most suitable values of the condition parameters that allow the proposed algorithm to obtain the best results are selected to be the default condition parameters provided in Table 1. These values are chosen in an objective way, and are able to yield good performance in enhancing edge features in a gradient image.

After all sub-images F_α have been processed using the proposed edge pixel enhancement processes, these sub-images are combined in the order of their decomposed sequences. Hence, the thin contour features are enhanced and the resulting edge feature enhanced image is denoted by F_q. Then, edge pixels can be obtained by thresholding F_q as discussed in the next section.

4 Bipolar oriented edge masks

Before applying the edge masks to the image F_q for removing the noisy pixels that are created by procedures described in the previous section, we have to threshold the entire image by a global threshold value to transform F_q into a binary image. The thresholding process is

$$F_t(i,j) = \begin{cases} 0 & \text{if } F_q(i,j) < T \\ 1 & \text{if } F_q(i,j) \geq T \end{cases} \tag{7}$$

where F_t is the binary edge image and T is the given threshold value. A proper threshold value can be obtained experimentally. A higher threshold value can extract more thin edges, but more noise points that do not really belong to any edge may also be extracted. A smaller threshold value is still able to extract the enhanced thin edges without producing a huge quantity of noisy pixels, but at the same time it may eliminate some really thin edges. We suggest using a value of T ranging from 20 to 30 as a good compromise for most images. On some occasions, however, if the suggested range of threshold values is not working well, the well-known method proposed by Otsu [15] can be used to determine an optimal values of T to transform F_q into a binary image. Otsu's thresholding method is a well-known thresholding method that can select a threshold value to separate the spread of foreground from background images. More detailed technical information about Otsu's thresholding method was given in [15].

Table 1: Edge pixel enhancement cases

Case	Condition			Update
	1	2	3	
Redundant background	$P_\alpha(i,j) < \mu_\alpha$	$\mu_\alpha < 2$	$\delta_\alpha < 2$	$P_\alpha(i,j) = 0$
Thin edge enhancement	$P_\alpha(i,j) > \mu_\alpha$ and $P_\alpha(i,j) < \mu_\alpha + 1.5 \times \delta_\alpha$	$\mu_\alpha < 2$	$\delta_\alpha < 2$	$P_\alpha(i,j) = P_\alpha(i,j)^2$
Intensive thin edge enhancement	$P_\alpha(i,j) > \mu_\alpha + 1.5 \times \delta_\alpha$ and $P_\alpha(i,j) < \mu_\alpha + 3 \times \delta_\alpha$	$\mu_\alpha < 2$	$\delta_\alpha < 2$	$P_\alpha(i,j) = P_\alpha(i,j)^3$
Thin edge in complex background	$P_\alpha(i,j) > \mu_\alpha + 1.5 \times \delta_\alpha$	$\mu_\alpha > 5$	$\delta_\alpha > 6$	$P_\alpha(i,j) = P_\alpha(i,j)^2$

We proposed five bipolar oriented edge masks, which are shown in Fig. 4. These edge masks are applied to the edge image F_t. The primary goal of applying these edge masks is to remove undesired noisy pixels in F_t. The masks are only applied to pixels that satisfy the following conditions:

1. The pixel is an edge point.
2. The sub-image F_α has mean value $\mu_\alpha < 3$ and standard deviation $\delta_\alpha < 3$, which are obtained from (5) and (6). This indicates that the sub-image belongs to the background or low-contrast regions in the original image F.

The scores of each mask applied to the pixels can be obtained by summing up the multiplications of the mask elements and their corresponding covered pixels in edge image F_t. If one of the scores is positive, then the corresponding pixel is considered to be a meaningful edge point; otherwise, the pixel is noise and should be removed from edge image F_t.

By applying these bipolar oriented edge masks, noisy pixels in image F_t can be easily removed, and the final edge image F_f is produced. In F_f, pixels with values equal to 1 are edge pixels, others are not. It should be noted that in Section 5, the experimental grey level values are intentionally inverted so that readers can recognise them more easily.

5 Experimental results

The performance of the proposed mathematical-morphology-based edge detection algorithm is evaluated in this section, and the comprehensive experimental results compared with other existing methods are also presented. The experimental results are presented in three categories: natural images, noise disturbed images and synthetic square images.

$$\begin{bmatrix} -2 & -2 & -2 & -2 & -2 & -2 & -2 \\ -2 & -2 & -2 & -2 & -2 & -2 & -2 \\ 1 & 1 & 1 & 1 & 1 & 1 & 1 \\ 2 & 2 & 2 & -2 & 2 & 2 & 2 \\ 1 & 1 & 1 & 1 & 1 & 1 & 1 \\ -2 & -2 & -2 & -2 & -2 & -2 & -2 \\ -2 & -2 & -2 & -2 & -2 & -2 & -2 \end{bmatrix}$$

a

$$\begin{bmatrix} -2 & -2 & 1 & 2 & 1 & -2 & -2 \\ -2 & -2 & 1 & 2 & 1 & -2 & -2 \\ -2 & -2 & 1 & 2 & 1 & -2 & -2 \\ -2 & -2 & 1 & -2 & 1 & -2 & -2 \\ -2 & -2 & 1 & 2 & 1 & -2 & -2 \\ -2 & -2 & 1 & 2 & 1 & -2 & -2 \\ -2 & -2 & 1 & 2 & 1 & -2 & -2 \end{bmatrix}$$

b

$$\begin{bmatrix} -1 & 1 & 2 & 1 & -2 & -2 & -2 \\ -1 & 1 & 2 & 1 & -1 & -2 & -2 \\ -1 & 1 & 2 & 1 & -1 & -2 & -2 \\ -2 & -1 & 1 & -2 & 1 & -1 & -2 \\ -2 & -2 & -1 & 1 & 2 & 1 & -1 \\ -2 & -2 & -1 & 1 & 2 & 1 & -1 \\ -2 & -2 & -2 & 1 & 2 & 1 & -1 \end{bmatrix}$$

c

$$\begin{bmatrix} 2 & 1 & -1 & -2 & -2 & -2 & -2 \\ 1 & 2 & 1 & -1 & -2 & -2 & -2 \\ -1 & 1 & 2 & 1 & -1 & -2 & -2 \\ -2 & -1 & 1 & -2 & 1 & -1 & -2 \\ -2 & -2 & -1 & 1 & 2 & 1 & -1 \\ -2 & -2 & -2 & -1 & 1 & 2 & 1 \\ -2 & -2 & -2 & -2 & -1 & 1 & 2 \end{bmatrix}$$

d

$$\begin{bmatrix} -2 & 1 & 1 & 2 & 1 & -2 & -2 \\ 1 & 1 & 1 & 2 & 1 & -2 & -2 \\ 1 & 1 & 1 & 2 & 1 & -2 & -2 \\ 2 & 2 & 2 & -2 & 1 & -2 & -2 \\ 1 & 1 & 1 & 1 & 1 & -2 & -2 \\ -2 & -2 & -2 & -2 & -2 & -2 & -2 \\ -2 & -2 & -2 & -2 & -2 & -2 & -2 \end{bmatrix}$$

e

Fig. 4 *Bipolar oriented edge masks*
a For angle 0
b For angle $\pi/2$
c For angles $3\pi/8$, and $5\pi/8$
d For angles $\pi/4$ and $3\pi/4$
e For corner edge

5.1 Natural images

Two natural images are utilised to demonstrate the performance of the proposed edge detection algorithm: 'Cameraman' and magnetic resonance image (MRI). These images have a common feature that they contain dark regions in the image. The contrast in these dark regions is so low that edge features in these regions are very difficult to detect. For the 'Cameraman' image shown in Fig. 5*a*, the cameraman is wearing a black coat that contains many important weak features. In this subsection, we will demonstrate that the proposed approach is actually capable of extracting smooth edges in the image. Several existing methods are also applied to the demonstration images for comprehensive comparison.

5.1.1 Cameraman: As mentioned above, the 'Cameraman' image contains many weak features on the coat, such as hand and pockets. The background also contains many features of buildings, but the grey level of these buildings is very similar to that of the sky. For comprehensive comparison, the Sobel edge detector [1], Prewitt edge detector [2], Canny edge detector [3] and the pure mathematical morphological dilation edge detector together with the proposed edge detector are applied to this image. The experimental results are shown in

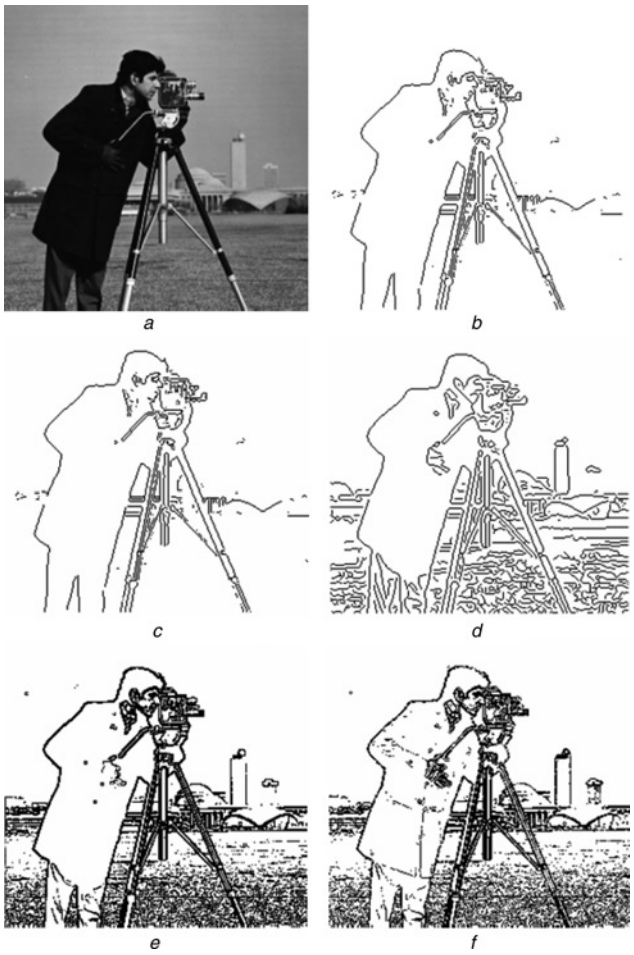

Fig. 5 *Performance of the proposed algorithm*
a Original image 'Cameraman'
b Edge detection results obtained by Sobel edge detector
c Edge detection results obtained by Prewitt edge detector
d Edge detection results obtained by Canny edge detector
e Edge detection results obtained by pure morphological edge detector
f Edge detection results obtained by the proposed edge detector

Fig. 5*b–f*. We can see that all previously proposed approaches can successfully extract the contour of the cameraman, but they failed to detect the outlines of the tower, and the pockets and buttons on the coat. However, the proposed algorithm did extract the smooth edges on the coat and in the background.

5.1.2 Magnetic resonance imaging: The MRI image shown in Fig. 6*a* contains many features of brain wrinkles and head cavities. The Sobel, Prewitt, Canny, pure morphological edge detectors and the proposed algorithms are applied to the image and the experimental results are shown in Fig. 6*b–f*. The conventional approaches are unable to detect detailed features in the MRI image. The pure morphological approach produces a good edge detection performance, but many really thin edges are still unable to be detected. An inspection of the shown figure clearly indicates that performance of the proposed edge detector algorithm is superior to those of the traditional ones. Using our approach, all thin features in the MRI image are detected and have a strong intensity.

5.2 Noise disturbed images

In this work, noise was added to the tested images to demonstrate the robustness of the proposed algorithm. To remove noise in the image, a median filter was applied before the edge detection algorithm processed the image. The conceptual block diagram is illustrated in Fig. 7. However, the median filter also smoothes the image to some extent. Therefore, edge features in the noise-filtered image become weak and insensitive to edge detectors. In this paper, we demonstrate that the proposed edge detection algorithm can successfully extract edge features even when the image is noisy and filtered by the median filter (with 5×5 filter mask).

Two noise functions, Gaussian and salt-and-pepper, were used to interpolate noises in the tested images. Here, Gaussian noise was added to the 'Model' image, and salt-and-pepper noise was added to images 'Aquitaine' and 'Lena'. The experimental results are discussed in the following subsections.

5.2.1 Model: The image 'Model' shown in Fig. 8*a* contains a female model and has a background consisting of the shadows of the glass shutters. A Gaussian noise function was first added to the image (Fig. 8*b*), and then the image was filtered by a median filter (Fig. 8*c*). It is clearly seen that the filtered image is blurrier than the original image. For comprehensive comparison, the Sobel, Prewitt, zero-cross and LoG edge detectors were also applied to the image. The resulting images are sequentially shown in Fig. 8*d–g*. Fig. 8*h* shows the experimental results obtained with the proposed algorithm. The proposed algorithm apparently

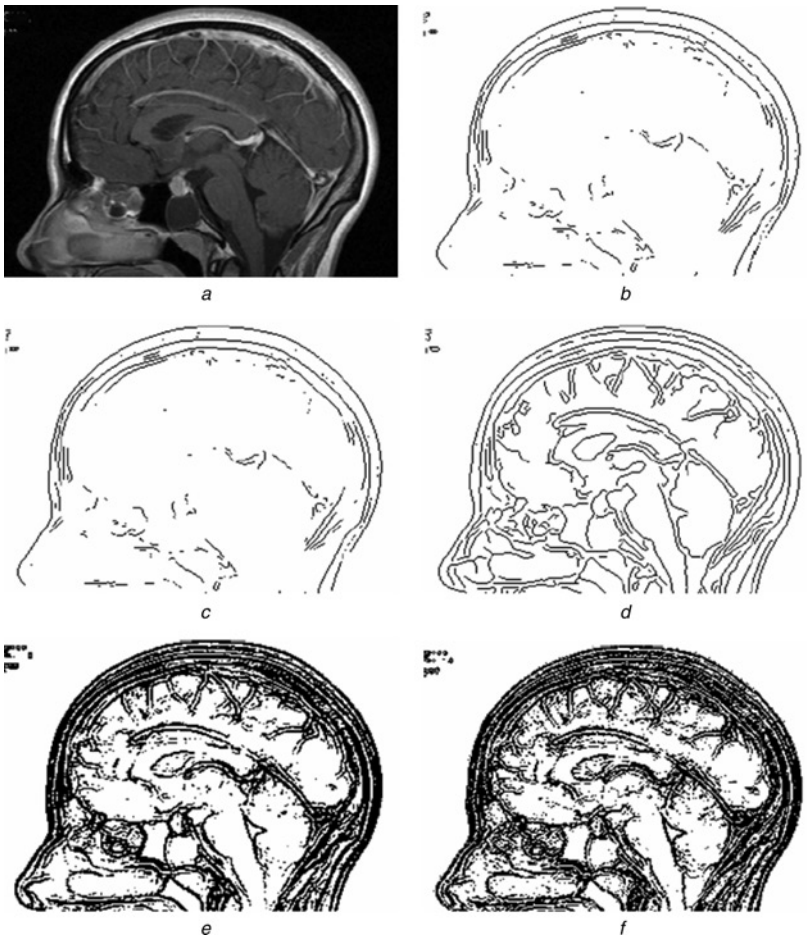

Fig. 6 *Performance of the proposed algorithm*

a Original MRI image
b Edge detection results obtained by Sobel edge detector
c Edge detection results obtained by Prewitt edge detector
d Edge detection results obtained by Canny edge detector
e Edge detection results obtained by pure morphological edge detector
f Edge detection results obtained by the proposed edge detector

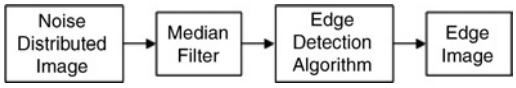

Fig. 7 *Block diagram for removing noises in an image*

outperforms the other approaches, and is capable of successfully extracting smooth edges in the image, such as boundary of hair and background shadows.

5.2.2 Aquitaine: As shown in Fig. 9*a*, the original image 'Aquitaine' is extremely dark, which makes the edge features very insensitive to any edge detector. For understanding of what is in the image, a contrast enhanced version of the image can be obtained by histogram equalisation, which is depicted in Fig. 9*b*. The image contains many farming fields and roads located between Bordeaux and Pyrenees in south western France. The salt-and-pepper noise function was added to the original image, and then we removed noise by median filtering. For comprehensive comparison, the Sobel, Prewitt, zero-cross and LoG edge detectors were also applied to the image. The experimental results obtained with the proposed algorithm is shown in Fig. 9*h*. The simulation result shows that the proposed algorithm is capable of extracting more boundaries of farming fields and roads, even if the contrast of the image is very low.

5.2.3 Lena: The image 'Lena' contains many interesting features, (Fig. 10*a*). The salt-and-pepper noise function was first added to the image (Fig. 10*b*), and then median filtering was used to remove noise (Fig. 10*c*). In this case, the Sobel, Prewitt, zero-cross and LoG edge detectors were also applied to the image. Fig. 10*d*–*g* shows the results. The experimental result obtained with the proposed algorithm is shown in Fig. 10*h*. The proposed algorithm can completely extract the boundaries of the hat and the arm of Lena. In particular, the facial features of Lena are successfully and fully extracted by the proposed algorithm.

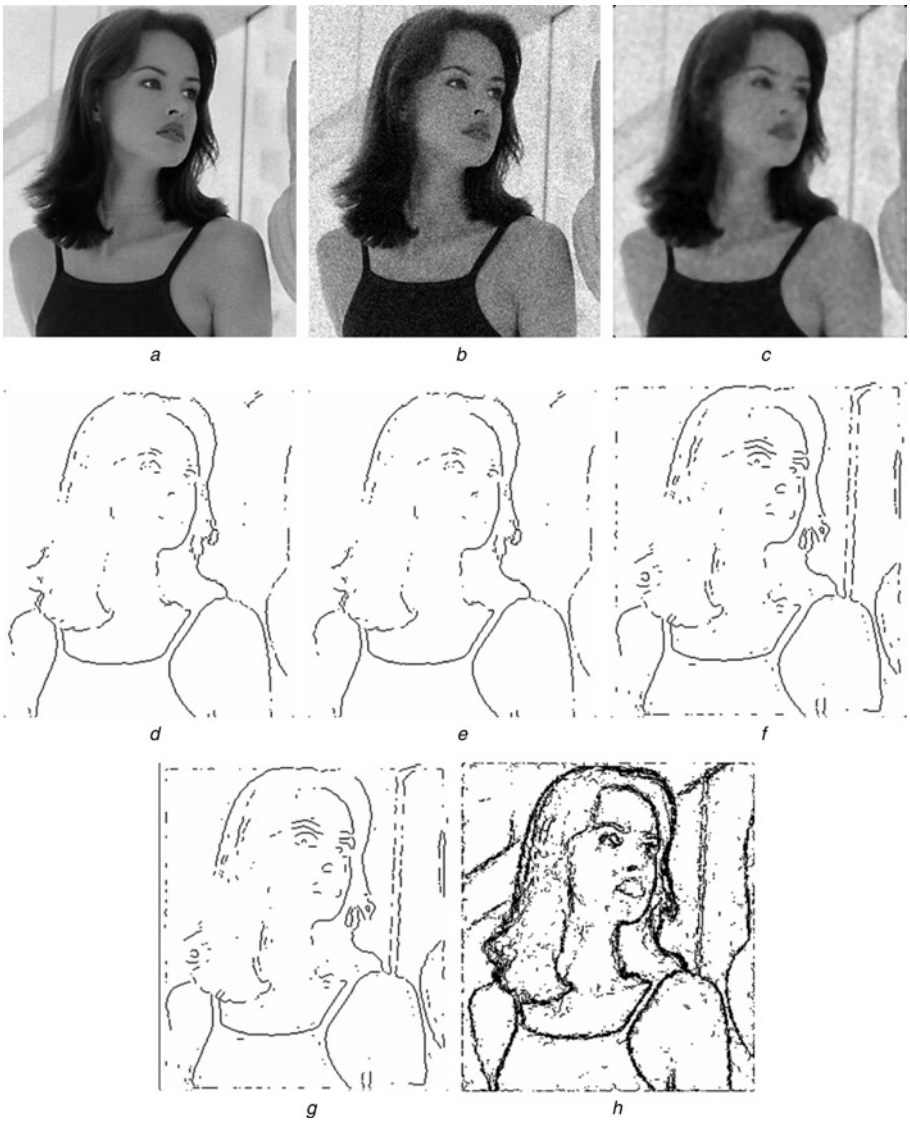

Fig. 8 *Noise disturbed images*

a Original image 'Model'
b After applying Gaussian noise function
c Filtered by median filter
d Edge detection results obtained by Sobel edge detector
e Edge detection results obtained by Prewitt edge detector
f Edge detection results obtained by zero-cross edge detector
g Edge detection results obtained by LoG edge detector
h Edge detection results obtained by the proposed edge detector

5.3 Synthetic square image

In this experiment, we used a synthetic ideal square image to test the performance of the proposed edge detector. The reason for using a synthetic image is that it allows us to measure the performances of different edge detectors with a known objective function. A 32×32 synthetic image containing a white square of 16×16 over a uniform black background was used to compare the performance and robustness of the proposed algorithm with those of other edge detectors.

To perform an objective measurement on all of the edge detectors, Pratt's figure of merit [13] was used to evaluate the performance of edge detectors. The figure of merit is

$$R = \frac{100}{\max(N_{\mathrm{I}}, N_{\mathrm{D}})} \sum_{i=1}^{N_D} \frac{1}{1 + \alpha d_i^2} \tag{8}$$

where d_i is the Euclidean distance between an extracted edge pixel and the nearest ideal edge pixel. α is the calibration constant and is set to $1/9$. N_{I} and N_{D} are the numbers of ideal edge points and extracted edge points, respectively. A larger value of R indicates better performance, with $R = 100$ meaning a perfect edge detection result. Two experiments were conducted and presented in this subsection. In these two experiments, a salt-and-pepper noise function with noise density of 0.07 and a Gaussian noise function with zero mean and variance of 0.02 were added to the ideal synthetic images, respectively. Then, the median filter was applied to the disturbed images to remove the noises of the images. At this stage, the synthetic images were blurred. The blurred images were utilised to conduct the experiments. For comparison, the simulation results with respect to the above-mentioned two cases are shown in sub-figures arranged with same order in Figs. 11 and 12, respectively.

For references, the utilised synthetic images are shown in Figs. 11*a* and 12*a*. Firstly, the salt-and-pepper noise function and the Gaussian noise function were added to the original images. The synthetic results are shown in Figs. 11*b* and 12*b*, respectively. After noise removal using median filtering, the blurred synthetic images were then utilised as

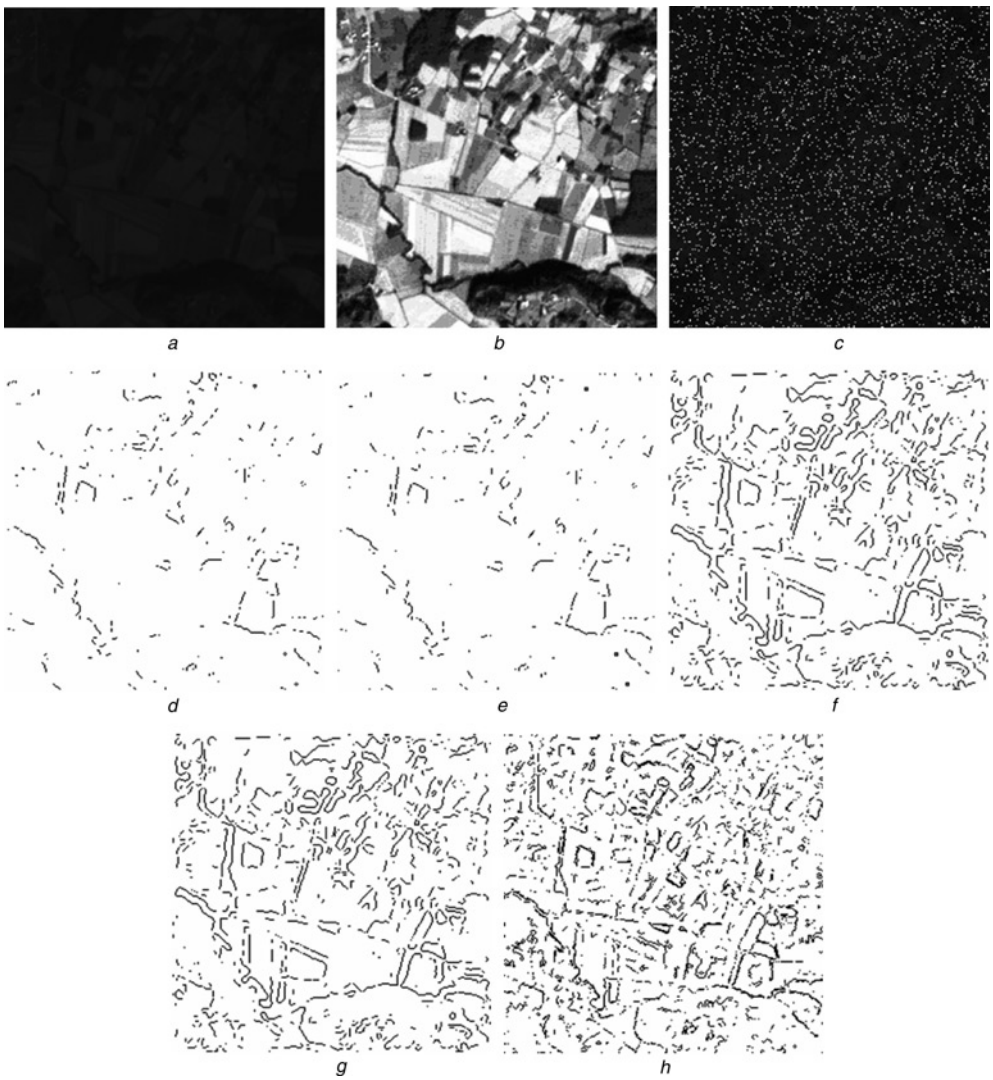

Fig. 9 *Noise disturbed images*

a Original image 'Aquitaine'
b Enhanced by histogram equalisation
c After applying salt-and-pepper noise function
d Edge detection results obtained by Sobel edge detector
e Edge detection results obtained by Prewitt edge detector
f Edge detection results obtained by zero-cross edge detector
g Edge detection results obtained by LoG edge detector
h Edge detection results obtained by the proposed edge detector

Fig. 10 *Noise disturbed images*

a Original image 'Lena'
b After applying salt-and-pepper noise function
c Filtered by median filter
d Edge detection results obtained by Sobel edge detector
e Edge detection results obtained by Prewitt edge detector
f Edge detection results obtained by zero-cross edge detector
g Edge detection results obtained by LoG edge detector
h Edge detection results obtained by the proposed edge detector

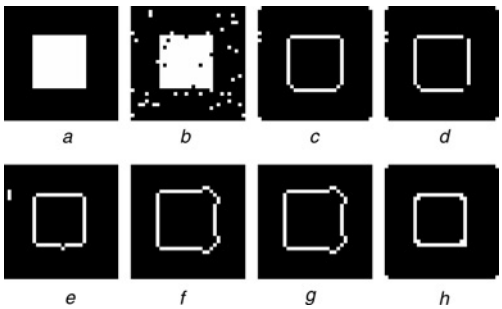

Fig. 11 *Noise disturbed images*

a Original image of synthetic ideal square image
b Resulting image after applying salt-and-pepper noise function
c Edge detection results obtained by Sobel edge detector
d Edge detection results obtained by Prewitt edge detector
e Edge detection results obtained by Canny edge detector
f Edge detection results obtained by zero-cross edge detector
g Edge detection results obtained by LoG edge detector
h Edge detection results obtained by the proposed edge detector

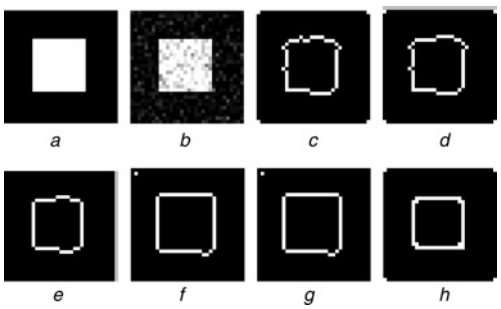

Fig. 12 *Noise disturbed images*

a Original image of synthetic ideal square image
b Resulting image after applying Gaussian noise function
c Edge detection results obtained by Sobel edge detector
d Edge detection results obtained by Prewitt edge detector
e Edge detection results obtained by Canny edge detector
f Edge detection results obtained by zero-cross edge detector
g Edge detection results obtained by LoG edge detector
h Edge detection results obtained by the proposed edge detector

Table 2: Measured values of Pratt's figure of merit of the proposed algorithm and some conventional edge detectors with respect to two different noise functions added to a synthetic ideal square images

	Pratt's figure of merit for edge detectors					
Tested cases	Sobel	Prewitt	Canny	Zero-cross	LoG	Proposed method
Case 1*	82.4	76.9	84.5	72.3	72.3	92.5
Case 2#	71.4	71.4	83.5	79.1	79.2	92.5

*Salt-and-pepper noise function with noise density = 0.07 is added into the tested image
#Gaussian noise function with mean = 0 and variance = 0.02 is added into the tested image

test targets. For comprehensive comparison, Sobel, Prewitt, Canny, zero-cross and LoG edge detectors were also applied to the synthetic square images, and the processed results are shown in Figs. 11*c*–*g* and 12*c*–*g*. The experimental results obtained by the proposed algorithm are shown in Figs. 11*h* and 12*h*. An examination of the results shown clearly indicates that the proposed edge detector is able to extract successfully the contour features in blurred synthetic images. The performances of Sobel and Prewitt edge detectors are similar, since they both are derivative edge detectors that shared the same principle of detecting contour features. The Canny edge detector provides performance slightly better than those of derivative edge detectors. As for zero-cross and LoG edge detectors, we observe that both of them can detect smooth edges. However, these two detectors have some defects in detecting contour features in the corner of the synthetic square, which are shown in Figs. 11*f* and 12*g*. Comparing with these widely utilised edge detection algorithms, the proposed approach is more robust against noise disturbed images. The results produced by the proposed method are very firm and clear.

Finally, Pratt's figures of merit applied to these edge detection algorithms for the synthetic square image are summarised in Table 2. From the table, it can be seen that Pratt's figure of merit achieved by the proposed algorithm was 92.5, which is significantly superior to values obtained by the other conventional approaches. This again verifies that the proposed algorithm outperforms other approaches overall.

6 Conclusions

A new edge detection algorithm based on the mathematical morphology has been proposed. The mathematical morphological edge detection algorithm is derived from the basic morphological operations. The input video frame is first processed by a morphological contrast enhancement operator and a dilation residue edge detection operator. The mathematical morphological dilation residue edge detector is then used in this algorithm for detecting the edge information, which can produce various strengths of edges in the image. The quad-decomposition edge enhancement process thresholding process and mask-based noise filter are also developed, and these new components are used to enhance thin edge features, extract edge points and filter out some meaninglessly noisy pixels, respectively. The proposed algorithm is able to detect the features in low-contrast regions, and preserve them as well as other apparent edges.

To demonstrate the performance of the proposed algorithm, comprehensive comparisons between well-known approaches and the proposed algorithm were carried out. Comparisons of edge detection accuracy have also been conducted using several noisy test images. The results indicate that the proposed algorithm is robust against noise or blurred images. Pratt's figure of merit achieved by the proposed algorithm, 92.5, is better than those obtained by the other edge detectors. Experimental results show that the proposed algorithm outperforms other edge detection methods in detecting detailed edge features and thin edge features in dark regions. Using the proposed algorithm, these thin edges can be preserved as well as other apparent edges even though the image is blurred or disturbed by noise.

7 Acknowledgments

The authors would like to thank the National Science Council of the Republic of China for financially supporting this research under Contract No. NSC 93-2213-E-002-133. The authors would also like to thank Dr Robert R. Bailey for his proof-reading of the manuscript and making a number of helpful suggestions.

8 References

1 Pratt, W.K.: 'Digital image processing' (Wiley Interscience, New York, 1978)
2 Nalwa, V.S.: 'A guided tour of computer vision' (Addison-Wesley, Reading, MA, USA, 1993)
3 Gonzalez, R.C., and Wintz, P.: 'Digital image processing' (Addison-Wesley, Reading, 1992)
4 Serra, J.: 'Image analysis and mathematical morphology' (Academic, New York, 1982)
5 Trujillo, A.: 'Thin edge detector'. Proc. Int. Conf. on Image Analysis and Processing, 1999, pp. 1051–1054
6 Chen, T., Wu, Q.H., Rahmani-Torkaman, R., and Hughes, J.: 'A pseudo top-hat mathematical morphological approach to edge detection in dark region', *Pattern Recognit.*, 2002, **35**, (1), pp. 199–210
7 Chanda, B., Kundu, M., and Vani Padmaja, Y.: 'A multi-scale morphologic edge detector', *Pattern Recognit.*, 1998, **31**, (10), pp. 1469–1478
8 Gong, W., Shi, Q., and Cheng, M.: 'Shape and image matching by use of morphology'. Proc. 11th IAPR Int. Conf. Pattern Recognition, 1992, pp. 673–676
9 Hirata, R. Jr., Barrera, J., Hashimoto, R.F., Dantas, D.O., and Esteves, G.H.: 'Segmentation of microarray images by mathematical morphology', *Real-Time Imaging*, 2002, **8**, (6), pp. 491–505
10 Lin, S.F., Chang, Y.L., and Chen, L.G.: 'Motion adaptive interpolation with horizontal motion detection for deinterlacing', *IEEE Trans. Consum. Electron.*, 2003, **49**, (4), pp. 1256–1265
11 Samet, H., and Webber, R.E.: 'Hierarchical data structures and algorithms for computer graphics.I. Fundamentals', *IEEE Trans. Comput. Graph. Appl.*, 1988, **8**, (3), pp. 48–68)
12 Samet, H., and Webber, R.E.: 'Hierarchical data structures and algorithms for computer graphics.II. Applications', *IEEE Trans. Comput. Graph. Appl.*, 1988, **8**, (4), pp. 59–75
13 Pratt, W.K.: 'Digital image processing' (John Wiley, New York, 1978)
14 Hsiao, Y.T., Chuang, C.L., Lu, Y.L., and Jiang, J.A.: 'Robust multiple objects tracking using image segmentation and trajectory estimation scheme in video frames', *Image Vis. Comput.*, 2006, **24**, (10), pp. 1123–1136
15 Otsu, N.: 'A threshold selection method from gray-level histograms', *IEEE Trans. Syst., Man., Cyber.*, 1979, **9**, pp. 62–66
16 Bangham, J.A., and Marshall, S.: 'Image and signal processing with mathematical morphology', *Electron. Commun. Eng. J.*, 1998, **10**, (3), pp. 117–128